

Kinetic energy dependence of $\text{Al}^{++}\text{O}_2 \rightarrow \text{AlO}^{++}\text{O}$

M. E. Weber, J. L. Elkind, and P. B. Armentrout

Citation: *The Journal of Chemical Physics* **84**, 1521 (1986); doi: 10.1063/1.450497

View online: <http://dx.doi.org/10.1063/1.450497>

View Table of Contents: <http://scitation.aip.org/content/aip/journal/jcp/84/3?ver=pdfcov>

Published by the [AIP Publishing](#)

Articles you may be interested in

Reaction dynamics of $\text{Al} + \text{O}_2 \rightarrow \text{AlO} + \text{O}$ studied by a crossed-beam velocity map imaging technique: Vibrational state selected angular-kinetic energy distribution

J. Chem. Phys. **140**, 214304 (2014); 10.1063/1.4879616

Temperature Dependent Anomalous Hall Effects in DMS $\text{Zn}(\text{Fe}, \text{Al})\text{O}$ Epitaxial Thin Film

AIP Conf. Proc. **1349**, 1045 (2011); 10.1063/1.3606220

Bias voltage dependence of tunnel magnetoimpedance in AlO_x -based magnetic tunnel junctions

J. Appl. Phys. **109**, 07C718 (2011); 10.1063/1.3556755

Chemiluminescence of AlO

J. Chem. Phys. **63**, 1963 (1975); 10.1063/1.431530

Laser fluorescence study of AlO formed in the reaction $\text{Al} + \text{O}_2$: Product state distribution, dissociation energy, and radiative lifetime

J. Chem. Phys. **62**, 1824 (1975); 10.1063/1.430710



Kinetic energy dependence of $\text{Al}^+ + \text{O}_2 \rightarrow \text{AlO}^+ + \text{O}$

M. E. Weber, J. L. Elkind, and P. B. Armentrout^{a)}
Department of Chemistry, University of California, Berkeley, California 94720

(Received 24 September 1985; accepted 28 October 1985)

The endothermic reaction of Al^+ with O_2 is studied using a guided ion-beam apparatus. The reaction cross section is measured as a function of kinetic energy from 0 to 20 eV. The threshold energy for the reaction, E_0 , is determined from an empirical model to be 3.64 ± 0.04 eV. Phase space calculations of the cross section performed with E_0 as the only adjustable parameter yield a similar result, $E_0 = 3.60 \pm 0.02$ eV, and predict the absolute magnitude of the reaction cross section within experimental error. We conservatively quote the threshold energy as 3.62 ± 0.12 eV which is somewhat higher than the thermodynamic threshold calculated using literature thermochemistry, 3.40 ± 0.16 eV. This may indicate that a slight barrier to the reaction exists, or that AlO^+ is produced in an excited state, or that the literature thermochemistry needs revision. Our results suggest $D_0^0(\text{AlO}^+) > 1.50 \pm 0.12$ eV and $\text{I.P.}(\text{AlO}) < 9.75 \pm 0.13$ eV.

INTRODUCTION

The gas-phase oxidation of metal atoms is of interest due to its importance in atmospheric chemistry,¹ in the development of new laser systems, and in the determination of metal oxide thermochemistry. Such reactions have also been useful model systems for the applicability of various statistical theories of reaction dynamics.^{2,3} Aluminum and its oxides have been particularly well studied both in neutral⁴⁻¹⁰ and ionic^{11,12} chemical studies. In the present study, we focus on the endothermic gas-phase ion-molecule reaction,



Using guided ion beam techniques, we have measured the reaction cross section as a function of kinetic energy. Similar experiments have been conducted previously by Rutherford and Vroom (RV)¹¹ and by Murad.¹² Including the present work, reaction (1) becomes one of the most well-studied endothermic reactions.

Our interest in this system centers on an evaluation of the translational energy dependence of the reaction cross section. Both RV and Murad have noted that reaction (1) has a threshold very near that expected from literature thermochemistry. This makes this reaction an attractive system to evaluate models of endothermic reactions and test the ability of these models and experiments to provide quantitative thermochemical data. By using empirical models, Armentrout *et al.*¹³ analyzed the data of RV and found that the line-of-centers (LOC) model¹⁴ provided a reasonable fit to the data and a threshold in agreement with the literature. We have recently begun using statistical models, in particular, the phase space theory of chemical kinetics,^{15,16} to perform similar analyses of a number of ion-molecule reactions. Most of these have involved reactions of atomic ions with H_2 . These cross sections typically rise rapidly from threshold and are modeled reasonably well by phase space theory^{17,18} and often by the LOC model.¹⁷⁻¹⁹

The applicability of phase space theory to reaction (1) is unclear. On one hand, the long-range attractive forces intrinsic to ion-molecule reactions help ensure that activation

barriers are small or nonexistent, and that loose transition states exist for both entrance and exit channels. On the other hand, phase space theory assumes that a strong-coupling collision, which results in complex formation, occurs if this barrier is surmounted. In general, a collisional complex which is long lived relative to a rotational period and perhaps to vibrational periods would have strong coupling. However, reaction (1) is highly endothermic and involves only three atoms. This suggests that at the energies necessary to drive the reaction, the AlO_2^+ intermediate will not be terribly long lived and the reaction will be direct.

POTENTIAL ENERGY SURFACES

One interesting facet of reaction (1) that has not been previously discussed is the nature of the reactive potential energy surface. It is complicated by the existence of several low-lying states of AlO^+ . While no experimental data are available, calculations by Schamps²⁰ predict a ground state of $^3\Pi$, with a $^1\Sigma^+$ state at 300 cm^{-1} (0.04 eV) and a $^1\Pi$ state at 2250 cm^{-1} (0.28 eV). As a comparison, similar calculations performed on the isoelectronic species, MgO , predict that the $^1\Sigma^+$ state, the experimentally determined ground state, lies 2360 cm^{-1} below the $^3\Pi$ state.²¹ For AlO^+ , the $^3\Pi$ or $^1\Sigma^+$ is probably the ground state, but the accuracy of the calculations, $\sim 1000 \text{ cm}^{-1}$,²¹ does not permit a definitive prediction of which is in fact the ground state.

Determination of which AlO^+ states can actually be produced from ground state reactants, $\text{Al}^+(^1S_g) + \text{O}_2(^3\Sigma_g^-)$, requires consideration of spin and angular momentum correlation rules. Table I shows the possible states of the AlO_2^+ intermediate which can be formed from the reactants and the various product channels in $C_{\infty v}$, C_{2v} , and C_s symmetries.²² These correlations predict that if $C_{\infty v}$ symmetry is maintained, both $\text{AlO}^+(^3\Pi)$ and $\text{AlO}^+(^1\Sigma^+)$ can be formed via a $^3\Sigma^-$ intermediate. In C_{2v} and C_s symmetries, this pathway is maintained, but now the intermediates are 3A_2 and $^3A''$, respectively. Thus, production of either the $^3\Pi$ or $^1\Sigma^+$ state conserves both spin and angular momentum.

Figure 1 displays the potential energy diagram for reac-

^{a)} Presidential Young Investigator, 1984-1989.

TABLE I. Spin and angular momentum correlations

Channel	Intermediate states			
	Spin	$C_{\infty v}$	C_{2v}	C_s
$\text{Al}^+(^1S_g) + \text{O}_2(^3\Sigma_g^-)$	3	Σ^-	A_2	A''
$\text{AlO}^+(^3\Pi) + \text{O}(^3P_g)$	5,3,1	Σ^+	A_1	A'
	5,3,1	Σ^-	A_2	A''
	5,3,1	Π	$B_1 + B_2$	$A' + A''$
	5,3,1	Δ	$A_1 + A_2$	$A' + A''$
$\text{AlO}^+(^1\Sigma^+) + \text{O}(^3P_g)$	3	Σ^-	A_2	A''
	3	Π	$B_1 + B_2$	$A' + A''$

tion (1).^{20,23} It shows that the ground state reactants, $\text{Al}^+(^1S_g) + \text{O}_2(^3\Sigma_g^-)$, correlate with the separated atoms, $\text{Al}^+(^1S_g) + 2\text{O}(^3P_g)$, as does one product channel, $\text{AlO}^+(^3\Pi) + \text{O}(^3P_g)$. On the other hand, the product channel, $\text{AlO}^+(^1\Sigma^+) + \text{O}(^3P_g)$, correlates with $\text{Al}^+(^1S) + \text{O}(^1D_g) + \text{O}(^3P_g)$, which in turn correlates with an excited state of reactants, $\text{Al}^+(^1S_g) + \text{O}_2(^3\Sigma_u^-)$. We conclude that the primary product channel is the diabatically favored process, $\text{AlO}^+(^3\Pi) + \text{O}(^3P_g)$. Formation of $\text{AlO}^+(^1\Sigma^+)$ from ground-state reactants could possibly proceed via a curve crossing which would most likely occur in the exit channel. Calculations on this region have not been performed but would be quite useful.

No spectroscopic or theoretical information is available for the intermediate species, AlO_2^+ ; however, it has 14 valence electrons and in analogy with NCN can be expected to be linear with a $^3\Sigma_g^-$ ground state.²³ Based on the correlation rules discussed above, this state is accessible to both the reactants and the products. AlO_2^+ is apparently stable having

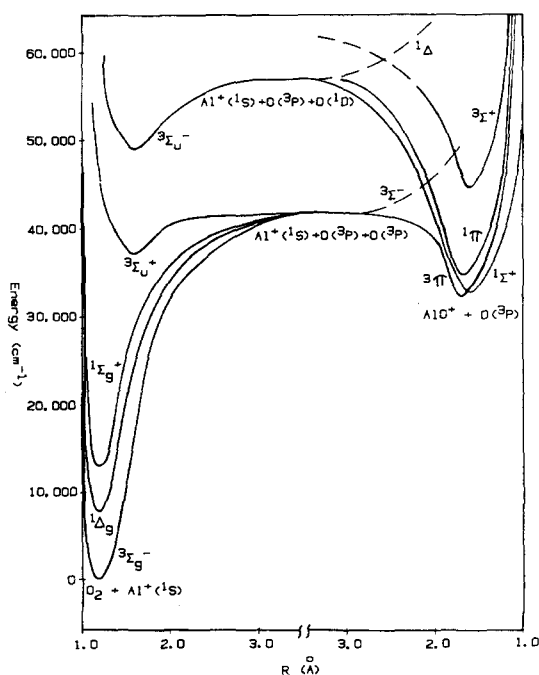


FIG. 1. Potential energy surfaces for reaction (1) assuming a single state for reactant Al^+ and for product O . The potential curves on the left are of O_2 (Ref. 23), while those on the right are of AlO^+ , obtained from SCF calculations (Ref. 20).

been observed in the electron impact ionization spectrum of the vapor over alumina.^{7,8} A value of 10 ± 1 eV was obtained for I.P. (AlO_2). In addition, Cornides and Gal⁴ have observed AlO_2^+ in a spark ion source containing alumina. Furthermore, preliminary studies in our laboratory have produced AlO_2^+ from sequential reactions between Al^+ and N_2O . The exothermicity for forming the intermediate, AlO_2^+ , from $\text{Al}^+ + \text{O}_2$ is 1.3 ± 1 eV.²⁴ This shallow well indicates that the formation of a long-lived complex is at least feasible. The fact that the well is less than half the reaction endothermicity implies that the lifetime of such a complex is probably less than a rotational period at the energies required to observe reaction (1).

EXPERIMENTAL

The ion beam apparatus and experimental techniques used in this work are described in detail elsewhere.²⁵ Mass analyzed Al^+ ions with well-defined translational energies are allowed to react with O_2 in a gas cell. Unreacted Al^+ ions and AlO^+ product ions undergo mass analysis and are detected using ion counting techniques. The problem of secondary ion collection losses, which is common in conventional beam-gas experiments, is essentially eliminated by the use of the ion beam guide technique.²⁶ This technique also permits low ion kinetic energies (< 0.1 eV) and provides routine energy analysis. Our ability to accurately calibrate the absolute energy scale using this technique has now been confirmed by several experiments.^{18,19,25} They demonstrate that the uncertainties are less than ± 0.1 eV lab (0.05 eV CM). Absolute magnitudes of the cross sections reported here have an uncertainty of $\pm 20\%$.

Aluminum ions are produced using a surface ionization source. In this source, a rhenium filament is resistively heated to ~ 2100 K and exposed to vaporized AlCl_3 or AlF_3 . If the ions equilibrate at the filament temperature, calculations show that virtually 100% of the Al^+ ions are in the 1S ground state. Less than $10^{-4}\%$ are in excited states.²⁷ The energy spread in the ion beam has a FWHM ranging from 0.35 to 0.70 eV lab (0.19 to 0.38 eV CM).

The two aluminum salts are introduced onto the filament differently. The more volatile AlCl_3 (sublimes at ~ 500 K) is contained in a heated reservoir external to the vacuum chamber. This source, which was used for all experiments described here, is subject to clogging, as the precise temperature range to which the reservoir must be heated is difficult to locate and maintain. In later experiments, AlF_3 (sublimes at ~ 1500 K) proved to be a more reliable source. Here, AlF_3 is contained in an oven immediately adjacent to the filament. This oven is wrapped in wire which is resistively heated to high temperatures (probably approaching 1000 K).

The threshold region obtained from the beam-gas geometry is less sharply defined than that from a crossed-beam apparatus. This is due to the random thermal motion of the reactant molecules in the gas cell, which creates a distribution of interaction energies for a given nominal ion energy. Since the beam is directional, and thus less random, this energy distribution is narrower for crossed-beam geometries. In either case, this so-called Doppler-broadening effect

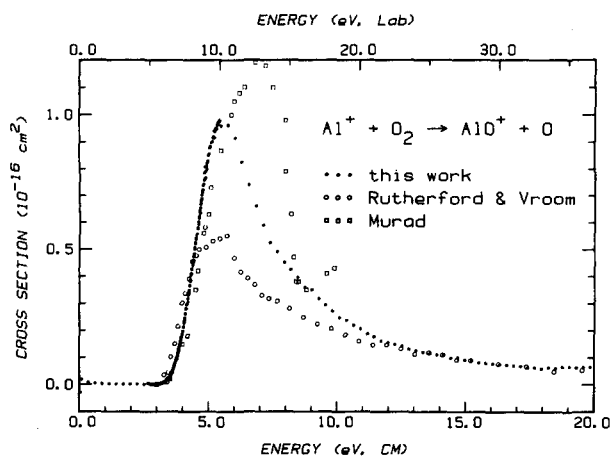


FIG. 2. Cross section for reaction (1) as a function of relative translational energy (lower scale) and laboratory energy (upper scale). The present data (points) are compared with literature results as reported by Rutherford and Vroom (open circles) and Murad (open squares).

results in an apparent threshold energy which is lower than the true threshold.²⁸ We account for this effect by convoluting a trial function for the true cross section with the target gas and ion beam energy distributions²⁹ before comparison with the experimental cross section.

RESULTS

The total cross section of reaction (1) is shown in Fig. 2 as a function of relative translational energy. As expected for an endothermic reaction, the cross section is zero until the apparent threshold energy, about 3 eV. The cross section reaches a maximum value of 1 \AA^2 at $\sim 5.5 \text{ eV}$, slightly above the O_2 dissociation energy [$D_0^0(\text{O}_2) = 5.115 \text{ eV}^{30}$]. Beyond this energy, the cross section declines due to the onset of the dissociation reaction,



Also shown in Fig. 2 are results from other researchers. RV¹¹ used a crossed-beam apparatus to investigate reaction (1). Near threshold, the magnitude of RV's cross section is comparable to ours. However, above 4.0 eV, it levels off to reach a peak magnitude which is approximately half that of ours. This is presumably due to the collection system of RV, in which product ions are collected only in the direction of the Al^+ beam. At higher energies, product ions could be scattered from this direction and not collected. Furthermore, RV's threshold data lie approximately 0.2 eV below ours, outside the limits of our energy scale uncertainty. This is surprising since the crossed-beam system has less energy broadening and thus would be expected to have an apparent threshold higher in energy compared with our beam-gas geometry. The discrepancy is presumably due to an error in the energy scale of RV. This may have been caused by the extraction field used to collect secondary ions. Alternatively, contact potentials or similar effects may have introduced errors in the calibration performed using retarding potential measurements.

The results of Murad,¹² obtained with a beam-gas system, are also shown in Fig. 2. The threshold data here either lie higher in energy compared with our data or slightly lower

in absolute magnitude. Murad measured the ion beam energy using conventional retarding potential analysis and justified the accuracy of his energy scale by noting that his apparent threshold (uncorrected for Doppler broadening) was consistent with the endothermicity calculated from available literature thermochemistry. The cross-section magnitude measured by Murad is comparable to our data considering his experimental uncertainty of 50%. This is reasonable since Murad's apparatus used a hemispherical grid extractor system designed for high collection efficiency. At higher energies, Murad's data fall off extremely fast and are incompatible with our results.

Threshold behavior

A value for the translational threshold energy, E_T , is found by fitting the data with an empirical model for the cross section, σ , as a function of relative translational energy, E . The general form for the model is

$$\sigma = \sigma_0(E - E_T)^n / E^m, \quad (3)$$

where σ_0 , n , and m are energy independent adjustable parameters. Various models for atom-diatom reactions predict values for m of 0.0, 0.5, 1.0, 1.5, 3.0, and n , with n ranging from 0.5 to 4.0.³¹ In light of these models, we explicitly evaluate the empirical model using all integral and half-integral values of m from 0 to 3, and m equal to n . Values of σ_0 , E_T , and n are allowed to vary freely until an optimum fit is obtained (as determined from nonlinear least-squares regression analysis). Prior to comparison with the data, the empirical models are convoluted with target gas and ion beam energy distributions to account for Doppler broadening. In all optimizations performed here, the model is fit to the data from below threshold to at least 4.85 eV, slightly below the onset of product dissociation.

Five sets of data taken over a nine-month period are analyzed. These include two threshold scans from 0 to almost 6 eV and three scans from 0 to 20 eV. Analysis of the

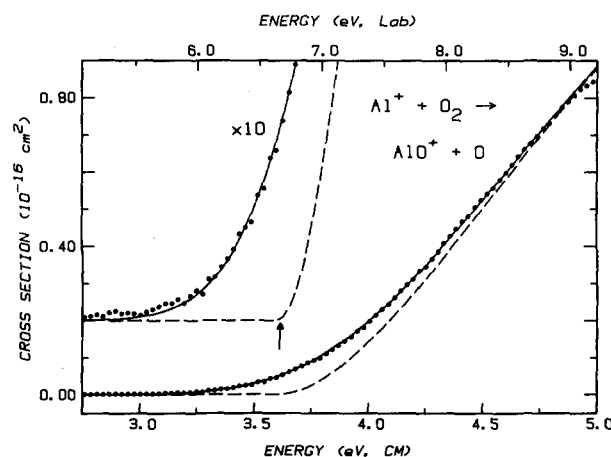


FIG. 3. Cross section for reaction (1) as a function of relative translational energy (lower scale) and laboratory energy (upper scale). The experimental data (points) are compared with the empirical model (broken line) using $m = 3.0$, $n = 2.0$, and $E_T = 3.61 \text{ eV}$ (shown by the arrow) and with the convolution of this model over the experimental energy distribution (solid line). The inset shows the data and fits expanded by a factor of 10 and offset from zero.

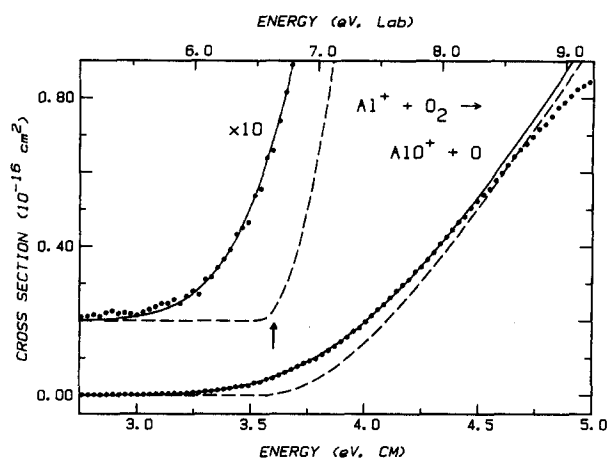


FIG. 4. Cross section for reaction (1) as a function of relative translational energy (lower scale) and laboratory energy (upper scale). The data (points) are compared to the phase space calculation (broken line) performed with the parameters given in Table II and $E_0 = 3.60$ eV (shown by the arrow) and to the convolution of this calculation over the experimental energy distribution (solid line). The phase space cross sections are reduced by 15.8%. The inset shows the data and calculations expanded by a factor of 10 and offset from zero.

two threshold scans should yield more precise thermochemical results due to the higher density of data in the threshold region. These five scans have been merged into one composite set of data shown in Figs. 3 and 4.

For all values of m , values of n and E_T could be found which fit the data well. Higher values of m result in a lower E_T , but the range of E_T 's for a given data set is < 0.13 eV. The average E_T of all these fits for all sets of data is 3.64 ± 0.04 eV, while the composite data file has an E_T of 3.59 ± 0.04 eV. The best fit uses $m = 3.0$ and $n = 2.0 \pm 0.10$. With m and n held at these values, the average optimum E_T is 3.61 ± 0.05 eV, while for the composite data file, the optimum E_T is 3.60 eV. This fit is shown in Fig. 3. We conclude that the best value for E_T (and pooled estimate of error³²) resulting from the empirical model is 3.61 ± 0.04 eV.

To calculate E_0 , the threshold energy for reaction (1) at 0 K, the energy available in internal degrees of freedom of the reactants must be considered. As noted above, the Al^+ beam is pure ground state 1S . The O_2 reactant, however, is at 305 K. At this temperature, excited vibrational states are

negligible, but many rotational states are populated. With the average rotational energy taken as simply kT , 0.025 eV, the value of E_T derived above can be corrected to $E_0 = 3.64 \pm 0.04$ eV. We can also treat the rotational states explicitly through Eq. (4):

$$\sigma(E) = \sum_J g(J) \sigma(E, J), \quad (4)$$

J refers to a given rotational state of O_2 , $g(J)$ is the fraction of molecules in that state [$\sum g(J) = 1$], and $\sigma(E, J)$ is given by Eq. (3) with E_T equal to E_0 minus the rotational energy for that state. Statistical populations and equal reaction probabilities are assumed. This treatment yields an E_0 which is 0.026 eV greater than E_T , again 3.64 ± 0.04 eV.

Phase space calculations

According to phase space theory, the reaction cross section for forming a particular product is proportional to the probability of dissociation of the collisional complex into the given product channel. This probability of dissociation is defined as the fraction of the total phase space available to that channel. The phase space available to each channel is found by summing the rotational-orbital states and then convoluting over the vibrational states. The total reaction cross section is then calculated classically by integrating over the initial rotational energy distributions and the impact parameter. This classical expression for the cross section is given elsewhere.³³ Bowers and Chesnavich¹⁶ have developed programs to perform these calculations for atom-diatom reactions. We use these programs with minor modifications to calculate a theoretical cross section as a function of translational energy for reaction (1).

The parameters used in the phase space calculations are given in Table II. For the reactant channel, $\text{Al}^+(^1S) + \text{O}_2(^3\Sigma_g^-)$, the molecular constants are well known. However, the constants, w_E , $w_E x_E$, and B_E , for $\text{AlO}^+(^3\Pi)$ in the product channel are uncertain. The values shown are our best estimates obtained from examining several sources. Schamps gives theoretical values for these constants from SCF calculations.²⁰ Comparison of similar calculations on isoelectronic species to experimental results indicates w_E is generally between 9% and 12% too high.^{21,34,35} Another estimate places w_E for $\text{AlO}^+(^3\Pi)$ as intermediate between that of the isoelectronic species, MgO and AlN .³⁶ Table III provides a summary of the various

TABLE II. Constants used in phase space calculations.

	$\text{Al}^+(^1S) \rightarrow \text{O}_2(^3\Sigma_g^-)$	$\text{AlO}^+(^3\Pi) + \text{O}(^3P)$
Atom mass (amu)	26.981	16.00
Diatom mass (amu)	32.000	42.981
Neutral polarizability, $\alpha(\text{\AA}^3)$	1.57	0.802
Symmetry number, s	2	1
Reactive electronic surfaces, g	3	3
Total electronic surfaces, G	3	54
w_E (cm^{-1})	1580.361	820 ± 110
$w_E x_E$ (cm^{-1}) ^a	12.07	12.7 ± 3.2
B_E (cm^{-1})	1.4457	0.57 ± 0.06

^a A Morse oscillator is assumed.

TABLE III. Values for AlO^+ molecular constants.

B_E (cm^{-1}) ^a		w_E (cm^{-1})		Reference
$^3\Pi$	$^1\Sigma^+$	$^3\Pi$	$^1\Sigma^+$	
0.5808	0.6380	911	819	b
0.51	0.58	710	820	c
0.57	0.625	820	740	d

^a Calculated from r_E using $B_E = h/8\pi^2\mu(\Pi r_E)^2$.

^b Reference 20.

^c Reference 36.

^d From r_E 1% higher than and w_E 10% lower than values in Ref. 20 (see the text).

estimates for w_E for both AlO^+ ($^3\Pi$) and AlO^+ ($^1\Sigma^+$). An analysis of the values given for r_E shows that the SCF values are generally about 1% lower than experimental r_E 's.^{21,34,35} JANAF adopts r_E for AlO^+ ($^3\Pi$) as 0.1 Å longer than that of Al_2O .³⁶ Table III also gives a summary of the B_E values as calculated from estimates for r_E . Note that, within the limits of uncertainty, the constants for the $^3\Pi$ state are indistinguishable from the constants for the $^1\Sigma^+$ state. In phase space calculations, the state of a species is identified only through these constants and the number of reactive surfaces.³³ (The total number of surfaces is used only for the reaction channel.) Thus, since both product channels have three reactive surfaces, the phase space calculations are insensitive to which product state is actually formed. As discussed above, we assume AlO^+ is in the $^3\Pi$ state.

The final parameter necessary in the calculations is the activation or threshold energy for a particular channel. E_0 is the only freely adjustable parameter in the calculations performed here. For a given set of parameters, E_0 is optimized to within ± 0.01 eV by trial and error through comparison with the composite data file. Again, the calculations are convoluted with target gas and ion-beam energy distributions prior to comparison. A reasonably good fit to the composite data file is made with $E_0 = 3.645 \pm 0.005$ eV and the molecular constants listed in Table II.

To estimate the error due to uncertainty in the molecular constants of AlO^+ , phase space calculations are also performed for the upper and lower limits of these constants. These include Schamps' molecular constants which have a high value of both w_E and B_E and JANAF's constants which are both low values. The best fit of the calculations to the data uses both the high B_E and high w_E and yields the lowest E_0 , 3.63 eV. The poorest fit uses both low values of B_E and w_E and yields a higher E_0 , 3.69 eV. Further calculations show that, in general, an increase of 10% in w_E results in a decrease of approximately 0.01 eV in E_0 . Likewise a 10% increase in B_E decreases E_0 by about 0.02 eV. Increasing w_E and B_E also gives better fits at higher energies. Additional calculations obtained by holding B_E to the value of 0.57 cm^{-1} and simultaneously optimizing w_E and E_0 , and likewise by holding w_E to 820 cm^{-1} and optimizing B_E and E_0 result in very good fits. These calculations indicate that the best w_E with these restraints is about 985 cm^{-1} and the best B_E is about 0.63 cm^{-1} , and in both cases $E_0 = 3.62$ eV. Including only calculations which gave good fits to the cross-

section data, the average E_0 from phase space is 3.63 ± 0.02 eV.

All comparisons made above do not include a consideration of the 20% uncertainty in our absolute cross section magnitude. This can be taken into account by allowing the phase space calculations to be scaled to the data. This analysis shows that the shape or curvature of the phase space results are only slightly sensitive to the molecular constants of AlO^+ . Changes in these constants primarily affect the absolute magnitude. In all cases, the scaled calculations fit the experimental data better at higher energies. Allowing for the error in our absolute magnitude, further calculations performed with the parameters in Table II give the optimum E_0 as 3.60 ± 0.02 eV. This calculation, which has been reduced 15.8%, is shown in Fig. 4. We consider this E_0 to be the best value obtained from a phase space analysis.

High energy behavior

The behavior of reaction (1) in the decay region, above 6 eV, is shown in Fig. 2 and again in Fig. 5 on a log-log scale. The data is remarkably linear in this plot. Regression analysis shows that the three high-energy scans decrease as $E^{-2.4 \pm 0.3}$ over the range, 7 to 12 eV. Beyond 12 eV, the scan shown continues in this fashion while the others deviate from this behavior. One becomes less steep and falls off as $E^{-1.3}$ while the other becomes more steep, $E^{-3.0}$. The origin of these differences is unclear but may be due to erratic collection of products. At these high energies, product collection can be difficult due to the large product velocities.

The decay region of reaction (1) can also be described using a simple statistical model. This model, derived in the Appendix, provides an expression for the probability of dissociation of the product ion, $P_D(E'_K)$, where E'_K is the product translational energy. Included in the expression are f which is the fraction of the products' internal energy in the ionic product, p which depends on the number of active vibrations and rotations, and D which is the product bond

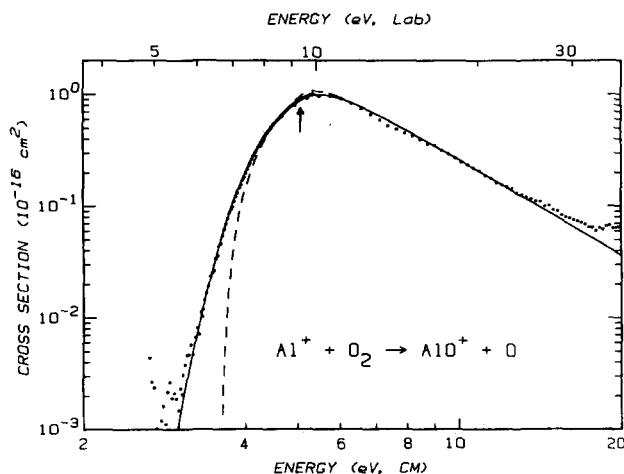


FIG. 5. Cross section for reaction (1) as a function of relative translational energy (lower scale) and laboratory energy (upper scale). The data (points) are compared to the high-energy model with $f=1.0$, $p=1.0$, $m=3.0$, $n=2.0$, and $E_T=3.61$ eV. The arrow indicates $D_0^0(\text{O}_2)$. The broken line and solid line are the unconvoluted and convoluted fits, respectively.

dissociation energy. For an atom-diatom system reacting via a loose transition state, both f and p must be unity. The cross section at high energies is given by Eq. (5), a modified version of Eq. 3:

$$\sigma(E) = \sigma_0 [(E - E_T)^n / E^m] [1 - P_D(E - E_T)]. \quad (5)$$

Equation (5) is applied to the cross section data with all values of m used in the threshold modeling and their corresponding values for n . E_T is set to 3.61 eV; the scaling factor σ_0 is optimized; and f and p are held to 1. (Values for f and p other than 1.0 were tested with various values of m , but none were found to fit the data well.) In general, a higher value of m results in a cross section with a steeper fall off. Thus, calculations with $m = 3.0$ (and $n = 2.0$) and $m = 2.5$ (and $n = 1.93$) fit the data remarkably well, while the other models fall off too slowly compared to the data. This again indicates higher values of m are more applicable to this system. Regression analysis shows the $m = 2.5$ fit falls off less rapidly than the data, while the $m = 3.0$ fit falls off slightly faster. This latter fit, which fits the data best in both the threshold and high-energy regions, is shown in Fig. 5.

DISCUSSION

Thermochemistry

The threshold energy derived from the present data is relatively insensitive to the model used for analysis. A broad range of empirical models yield an average E_0 of 3.64 ± 0.04 eV where the uncertainty accurately reflects the range of threshold values obtained. In excellent agreement with this value is the result of the phase-space analysis, $E_0 = 3.60 \pm 0.02$ eV. We conclude the best value of E_0 for our data is 3.62 ± 0.12 eV. The uncertainty, which includes the uncertainty in the absolute energy scale of ± 0.05 eV, is conservatively quoted as twice the pooled estimate of error.

As noted in the Introduction, it is believed that reaction (1) has a threshold near the thermodynamic limit.¹¹⁻¹³ This limit can be calculated from literature thermochemistry using Eqs. (6) and (7),

$$E_0 = D_0^0(\text{O}_2) - D_0^0(\text{AlO}^+), \quad (6)$$

$$D_0^0(\text{AlO}^+) = D_0^0(\text{Al-O}) + \text{I.P.}(\text{Al}) - \text{I.P.}(\text{AlO}). \quad (7)$$

$D_0^0(\text{O}_2) = 5.115 \pm 0.002$ eV³⁰ and $\text{I.P.}(\text{Al}) = 5.986$ eV³⁷ are well known, but the other quantities are somewhat uncertain. Various techniques have been used to determine $D_0^0(\text{AlO})$. Drowart³⁸ has reviewed and re-interpreted the more reliable determinations prior to 1973 and suggests $D_0^0(\text{AlO}) = 5.26 \pm 0.04$ eV. Additional measurements made since 1973 have been discussed by Pasternack and Dagdigian (PD).³ Most are found to be in excellent agreement with this value, although a few flame photometry determinations indicate a value higher by ≈ 0.1 eV. Using the values suggested by Drowart and PD yields an average value and pooled error of 5.26 ± 0.06 eV.

The most uncertain thermochemical value in the literature is $\text{I.P.}(\text{AlO})$. Ho and Burns⁷ measured the appearance potential of AlO^+ to be 9.5 ± 0.2 eV through electron impact of AlO over alumina at temperatures of ≈ 2200 – 2300 K. Hildenbrand⁶ used a similar technique to determine

$\text{AP}(\text{AlO}^+) = 9.53 \pm 0.15$ eV in this same temperature range. Hildenbrand suggests then that $\text{I.P.}(\text{AlO})$ is close to this value based on a comparison of his measured value for $\text{AP}(\text{SO}^+)$, 10.28 ± 0.02 eV, to a value of $\text{I.P.}(\text{SO}) = 10.34 \pm 0.02$ eV obtained by photoelectron measurements (PES).³⁹ The most recent value is $\text{I.P.}(\text{SO}) = 10.29 \pm 0.01$ eV,⁴⁰ in good agreement with the PES value. It is still unclear, however, whether the measured value of $\text{AP}(\text{AlO}^+)$ is influenced by hot bands. The average internal energy of the AlO at 2200 K is 0.39 eV.⁴¹ Depending on the strength of hot bands, the measured appearance potentials may underestimate the 0 K ionization potential by some fraction of this internal energy. Indeed, Schamps²⁰ provides a value for $\text{I.P.}(\text{AlO})$ of 10.1 ± 0.1 eV from SCF calculations, and other less precise measurements^{8,9,42} center around the value 9.7 ± 0.5 eV. Nevertheless, the best available estimate of $\text{I.P.}(\text{AlO})$ is 9.53 ± 0.15 eV.

Combining these literature values using Eq. (7) yields $D_0^0(\text{AlO}^+) = 1.71 \pm 0.16$ eV. The literature threshold energy calculated from Eq. (6) is therefore $E_0 = 3.40 \pm 0.16$ eV. Our experimentally determined E_0 , 3.62 ± 0.12 eV exceeds the value calculated from the literature by 0.22 eV, which is just inside the limits of the combined uncertainties. Several possible explanations for this discrepancy exist. The first concerns the uncertainty of the ground state of AlO^+ . The literature thermochemistry may be based on a different state of AlO^+ than is produced in reaction (1), the $^3\Pi$ state as discussed above. This would imply that the ground state of AlO^+ is $^1\Sigma^+$ and that the $^3\Pi$ state is 0.22 ± 0.20 eV ($\approx 1800 \pm 1600$ cm^{-1}) above this. While this differs quite a bit from the calculated energies of these states (0.04 eV favoring the $^3\Pi$ state),²⁰ these states have electron correlation effects which are very different. The calculated values include these effects using semiempirical estimates which could easily be in error by 1000 cm^{-1} .

A second explanation is that a barrier to the reaction may exist. It is hard to understand why such a barrier would exist in the exit channel considering that the products, AlO^+ ($^3\Pi$) and O (3P_g), are ionic and open shell species and therefore would be expected to be everywhere attractive. However, interactions among the several low-lying electronic states of AlO^+ could conceivably result in an exit channel barrier. A more likely place to find a reaction barrier is in the entrance channel since the reactant ion, Al^+ (1S), has a very stable closed shell $3s^2$ electron configuration. However, the observed threshold implies that the barrier for insertion of Al^+ into O_2 is very large, ≈ 3.6 eV.⁴³ Such a large barrier is inconsistent with the ability of the phase space calculations to accurately predict both the shape and magnitude of the experimental cross sections. Calculations on the potential energy surfaces of reaction (1) would be very useful in evaluating the likelihood of these barriers.

The third possible explanation is that the literature thermochemistry needs revision. Presuming that there is no barrier to reaction in excess of the endothermicity, our measured threshold energy can be used to derive several thermochemical values of interest. However, because the possibility of a barrier cannot be excluded, this threshold is most conservatively viewed as an upper limit to the thermo-

dynamic threshold. Thus, our results provide a lower limit to $D_0^0(\text{AlO}^+)$ of 1.50 ± 0.12 eV, and when combined with the literature value for $D_0^0(\text{AlO})$ of 5.26 ± 0.06 eV, yield an upper limit on I.P.(AlO) of 9.75 ± 0.13 eV. This seems a reasonable figure compared to the literature value of 9.53 ± 0.15 eV, especially when hot-band effects are considered. Alternatively, if the literature value for I.P.(AlO) is accepted, our results imply a lower limit of 5.02 ± 0.19 eV for $D_0^0(\text{AlO})$. This tends to support the lowest values obtained by other methods.

Previous results

The results of the empirical analysis here are in contrast to the conclusions of a similar analysis performed by Armentrout *et al.* (AHB)¹³ on the data of RV. There, the best fit used the line-of-centers (LOC) model ($n = m = 1.0$) and $E_T = 3.38$ eV. However, the main criterion for evaluating the "best" fit was the ability to reproduce the literature threshold energy, then believed to be 3.45 ± 0.16 eV. As discussed above, we now believe the data of RV has an inaccurate energy scale. Evaluation of the data of RV using any of the empirical models which also reproduce our data, yields thresholds which indicate RV's energy scale is ≈ 0.45 eV lower than ours. All these models (unconvoluted) are consistent with the shape of RV's data in the threshold region. In contrast, the LOC model cannot adequately describe our experimental results. The implication of this is that the other bond energies derived by AHB may be too low due to the erroneous use of the LOC model. If we also reevaluate Murad's data using our empirical models, we find that his energy scale is higher than ours by only 0.06 eV. This error is well within the mutual energy scale uncertainties.

Energy dependence

Not only do the empirical models and phase space model provide threshold energies in good agreement with one another, but the shapes of these model cross sections are nearly identical from threshold to about 5 eV, Figs. 3 and 4. This lends confidence to the unconvoluted cross sections derived here. It seems particularly significant that the phase space model yields the correct absolute magnitude within experimental error. While it is possible that this is merely fortuitous, this agreement suggests that the phase space model is indeed applicable to this system. This implies that a deep potential well in the reaction surface is not required for strong coupling of reaction channels and that there are no large barriers in the entrance and exit channels. It is not inconsistent with a small exit barrier or the formation of an excited state of AlO^+ .

We have previously observed that the phase space model accurately reproduces the cross sections of other highly endothermic atom-diatom ion-molecule reactions.^{17,18} All of these other reactions involve H_2 and are found to rise rapidly from threshold in contrast to the cross section for reaction (1). Model phase space calculations indicate that this slower rise is due to the cumulative effects of having smaller changes in the vibrational frequency, the rotational constant, and the reduced mass. Thus, the dominant effect

which differentiates reaction (1) from reactions with H_2 is the mass of the oxygen compared with that of hydrogen. One implication of this is that while the line-of-centers form of Eq. (3), $n = m = 1$,¹⁴ may be a useful empirical model for the threshold behavior of reactions with H_2 , it is not a good model for reactions with heavier molecules. In general, we expect that the LOC function may only be useful for interpreting the threshold behavior for production of HL in $\text{H} + \text{LL}$ and $\text{H} + \text{LH}$ systems (where H represents a heavy atom or molecule and L represents a light atom or molecule).

As mentioned above, the values of m [Eq. (3)] used in the empirical modeling were chosen because they had been predicted by one theoretical model or another. It is of interest to compare the values of n [Eq. (3)] derived empirically with those predicted by these models. From such comparisons, information concerning the reaction dynamics can possibly be obtained. For example, the leading term in the phase space model should yield $m = 0$ and $n = 1.25$ for ion-molecule reactions.^{15,16} Experimentally, we find that when $m = 0$, n does, in fact, equal 1.25 ± 0.17 in good agreement with the ability of the full phase space calculation to reproduce the data. Another theory predicts that when $m = 3$, n should be between 3 and 4 depending on the nature of the intermediate.⁴⁴ We find, however, that if $m = 3$ then n must be 2.0 ± 0.10 in order to fit the data. Likewise, for $m = 1.5$, theory⁴⁵ suggests $n = 2.5$ while experimentally we find $n = 1.65 \pm 0.17$. More interesting is the observation that if $m = 1$ then experimentally we find $n = 1.50 \pm 0.15$. Chesnavich and Bowers⁴⁶ have derived a model for translationally driven (direct) reactions using transition state theory and additional assumptions outlined by Marcus.⁴⁷ This model predicts m always equals 1 while the value of n depends on the nature of the transition state. For atom-diatom reactions, n equals 0.5 or 1 for a loose transition state⁴⁸; n equals 1.5 for a tight nonlinear transition state; and n equals 2 for a tight linear transition state. This comparison could be used to infer details of the transition state for reaction (1); however, the fact that both the statistical phase space theory and a direct reaction model can reproduce the shape of the cross section means that such agreement is not a definitive demonstration of the reaction dynamics. More convincing is that the phase space model reproduces both the shape and absolute magnitude of the experimental cross section. The direct model predicts a magnitude about 20 times larger than observed. Caution is obviously required when deriving dynamic information from the comparison of simple models with experimental cross sections.

ACKNOWLEDGMENTS

This work is supported by the National Science Foundation, Grant No. CHE-8306511. We would like to thank W. Chesnavich, M. Bowers, and M. Jarrold for providing access to their phase space programs.

APPENDIX: HIGH ENERGY DECAY

The decay regions of both exothermic and endothermic cross sections have been less studied than the low energy

regions. Here, we formulate a model which is based on a simple treatment of product translational energy distributions by Safron *et al.* (SWHT).⁴⁹ By energy conservation, such a distribution can be converted to a distribution of product internal energies, $E'_i = E' - E'_K$. By assuming that the product decomposes if E'_i exceeds the dissociation energy of the product, this distribution can in turn be converted into a dissociation probability.

SWHT give the distribution of product translational energies, E'_K , as

$$P(E'_K) = N_{vr}(E' - E'_K) A(E'_K), \quad (\text{A1})$$

where $N_{vr}(E' - E'_K)$ is the density of active internal states in the transition state. $A(E'_K)$ is the fraction of these states which are actually attainable given the restraint of angular momentum in going from reactants to products. Klots⁵⁰ has pointed out that some of the assumptions made in deriving Eq. (A1) may be in serious error in some cases. The simple treatment here could be improved by avoiding these assumptions as discussed by Klots.

The probability of dissociation, P_D , is simply the integral of $P(E'_K)$ over all product kinetic energies which lead to ion dissociation normalized by the total distribution,

$$P_D = \int_0^{E'_K(\text{max})} P(E'_K) dE'_K / \int_0^{E'} P(E'_K) dE'_K. \quad (\text{A2})$$

Dissociation is assumed to occur when the internal energy of the ionic product exceeds its bond energy, D . The average fraction of the products' internal energy in the ionic product is defined as f . For the case of an atomic neutral product, f must equal 1. A more exact treatment of this problem could include a statistical distribution for f rather than an average value. Thus, dissociation will occur when $f(E' - E'_K) > D$ or equivalently, when $E'_K < (E' - D/f) = E'_K(\text{max})$.

Using expressions given by SWHT, one can show that for the case of endothermic ion-molecule reactions, A can be written simply as

$$A(E'_K) = (\mu'/\mu)(\alpha'E'_K/\alpha E_K)^{1/2}, \quad (\text{A3})$$

where μ is the reduced mass, α is the polarizability of the neutral, and primed and unprimed variables refer to products and reactants, respectively. This form for A depends on the assumption that the rotational angular momentum of the reactants and products is much less than the total orbital angular momentum which, therefore, does not change in the course of the reaction. Also note that the dependence on the reduced masses and polarizabilities will cancel in the expression for P_D , Eq. (A2).

The final quantity required is N_{vr} . Here, we use expressions in the classical limit such that

$$N_{vr}(E' - E'_K) \propto (E' - E'_K)^p, \quad (\text{A4})$$

where $p = s + r/2 - 1$ and s and r equal the number of active vibrations and rotations, respectively, in the transition state. The proportionality constant cancels in the expression for P_D and therefore is not specified here. Other, more accurate means could also be used to evaluate N_{vr} .⁵¹

Substituting Eqs. (A3) and (A4) into Eq. (A2) yields the final expression for the dissociation probability:

$$P_D = \frac{\int_0^{E'_K(\text{max})} (E' - E'_K)^p E_K^{1/2} dE'_K}{\int_0^{E'_K} (E' - E'_K)^p E_K^{1/2} dE'_K}. \quad (\text{A5})$$

The integrals may be solved in closed form when p is integral or half-integral. The exact choice of p depends on whether the transition state (TS) is assumed to be loose or tight. For an atom-diatom reaction ($f = 1$), a loose TS means that $s = 1$, $r = 2$, and $p = 1$; a tight nonlinear TS means $s = 2$, $r = 1$, and $p = 3/2$; a tight linear TS gives $s = 3$, $r = 0$, and $p = 2$. For $p = 1$ and $f = 1$, the result is particularly simple,

$$P_D = (1 - D/E')^{3/2} (1 + 3D/2E'). \quad (\text{A6})$$

Note that the thermodynamic threshold for dissociation occurs when P_D equals zero, i.e., when $E' = D$.

It might be noted that a previous treatment of the high energy behavior of reaction cross sections utilized a similar treatment to the one derived here.⁵² This treatment neglects the angular momentum constraints contained in Eq. (A3) by assuming that A was independent of energy. This simplifies the equations even further such that P_D is given by $1 - (D/fE')^{p+1}$ or for the loose TS atom-diatom case, $P_D = 1 - (D/E')^2$.

The application of these equations to experimental data is straightforward. The cross-section function for formation of the product ion is multiplied by the probability that the ion does not dissociate, $1 - P_D$. D is either well known or can be measured using the endothermicity of the reaction. Likewise, E' is assumed to be the difference in total reactant energy and threshold energy. The parameters, f and p , can be calculated *a priori* but may also be treated as variable parameters.

¹E. J. Murad, *Geophys. Res.* **83**, 5525 (1978).

²P. J. Dagdigian, H. W. Cruse, A. Schultz, and R. N. Zare, *J. Chem. Phys.* **61**, 4450 (1974).

³L. Pasternack and P. J. Dagdigian, *J. Chem. Phys.* **67**, 3854 (1977).

⁴I. Cornides and T. Gal, *High Temp. Sci.* **10**, 171 (1978).

⁵J. Drowart, G. DeMaria, R. P. Burns, and M. G. Inghram, *J. Chem. Phys.* **32**, 1366 (1960).

⁶D. L. Hildenbrand, *Chem. Phys. Lett.* **20**, 127 (1973).

⁷P. Ho and R. P. Burns, *High Temp. Sci.* **12**, 31 (1980).

⁸M. Farber, R. D. Srivastava, and O. M. Uy, *J. Chem. Soc. Faraday Trans.* **1**, **68**, 249 (1972).

⁹R. C. Paule, *High Temp. Sci.* **8**, 257 (1976).

¹⁰J. L. Gole and R. N. Zare, *J. Chem. Phys.* **57**, 5331 (1972).

¹¹J. A. Rutherford and D. A. Vroom, *J. Chem. Phys.* **65**, 4445 (1976).

¹²E. J. Murad, *Chem. Phys.* **77**, 2057 (1982).

¹³P. B. Armentrout, L. F. Halle, and J. L. Beauchamp, *J. Chem. Phys.* **76**, 2449 (1982).

¹⁴The LOC model is given by Eq. (3) with $n = m = 1$. R. D. Levine and R. B. Bernstein, *Molecular Reaction Dynamics* (Oxford University, New York, 1974), p. 46.

¹⁵J. C. Light, *J. Chem. Phys.* **40**, 3221 (1964); E. Nikitin, *Theor. Exp. Chem.* **1**, **83**, 90, 275 (1975).

¹⁶W. J. Chesnavich and M. T. Bowers, *J. Chem. Phys.* **68**, 901 (1978).

¹⁷J. L. Elkind and P. B. Armentrout, *J. Phys. Chem.* (in press).

¹⁸K. M. Ervin, J. L. Elkind, and P. B. Armentrout (work in progress).

¹⁹J. L. Elkind and P. B. Armentrout, *J. Phys. Chem.* **88**, 5454 (1984).

²⁰J. Schamps, *J. Chem. Phys.* **2**, 352 (1973).

- ²¹J. Schamps and H. Lefebvre-Brion, *J. Chem. Phys.* **56**, 573 (1972).
- ²²K. E. Shuler, *J. Chem. Phys.* **21**, 624 (1953).
- ²³G. Herzberg, *Spectra of Diatomic Molecules* (Van Nostrand Reinhold, New York, 1950), p. 446; *Electronic Spectra and Electronic Structure of Polyatomic Molecules* (Van Nostrand Reinhold, New York, 1966), p. 345.
- ²⁴Calculated from $D_0^0(\text{Al}^+-\text{O}_2) = -\text{I.P.}(\text{AlO}_2) + D_0^0(\text{Al}-\text{O}_2) + \text{I.P.}(\text{Al})$, where $D_0^0(\text{Al}-\text{O}_2) = 5.29 \pm 0.22$ eV (Ref. 36) and $\text{I.P.}(\text{Al}) = 5.986$ eV (Ref. 37).
- ²⁵K. M. Ervin and P. B. Armentrout, *J. Chem. Phys.* **83**, 166 (1985).
- ²⁶E. Teloy and D. Gerlich, *Chem. Phys.* **4**, 417 (1974).
- ²⁷The lowest lying excited state, 3P , is 4.651 eV above the ground state (Ref. 37).
- ²⁸P. J. Chantry, *J. Chem. Phys.* **55**, 2746 (1971).
- ²⁹C. Lifshitz, R. L. C. Wu, T. O. Tiernan, and D. T. Terwilliger, *J. Chem. Phys.* **68**, 247 (1978).
- ³⁰M. W. Chase, Jr., J. L. Curnutt, J. R. Downey, Jr., R. A. McDonald, A. N. Syverud, and E. A. Valenzuela, *J. Phys. Chem. Ref. Data* **11**, 926 (1982).
- ³¹See discussion in N. Aristov and P. B. Armentrout, *J. Am. Chem. Soc.* (in press).
- ³²G. E. P. Box, W. G. Hunter, and J. S. Hunter, *Statistics for Experimenters* (Wiley, New York, 1978), p. 319.
- ³³D. A. Webb and W. J. Chesnavich, *J. Phys. Chem.* **87**, 3791 (1983).
- ³⁴K. D. Carlson, K. Kaiser, C. Moser, and A. C. Wahl, *J. Chem. Phys.* **52**, 4678 (1970).
- ³⁵W. M. Huo, K. F. Freed, and W. Klemperer, *J. Chem. Phys.* **46**, 3556 (1967).
- ³⁶M. W. Chase, Jr., J. L. Curnutt, R. A. McDonald, and A. N. Syverud, *J. Phys. Chem. Ref. Data* **7**, 828, 830 (1978); D. R. Stull and H. Prophet, *Natl. Stand. Ref. Data Ser., Nat. Bur. Stand.* **37**, (1971).
- ³⁷W. C. Martin and R. Zalubas, *J. Phys. Chem. Ref. Data* **8**, 817 (1979).
- ³⁸J. Drowart, *Faraday Symp. Chem. Soc.* **8**, 165 (1974).
- ³⁹N. Jonathan, D. J. Smith, and K. J. Ross, *Chem. Phys. Lett.* **9**, 217 (1971).
- ⁴⁰J. M. Dyke, L. Golob, N. Jonathan, A. Morris, M. Okuda, and D. J. Smith, *J. Chem. Soc. Faraday Trans. 2* **70**, 1818 (1974).
- ⁴¹This value is calculated by explicitly averaging the rotational and vibrational energies, assuming Bottemann distributions (constants from Ref. 36). It is slightly greater than $2kT$.
- ⁴²S. Smoes, J. Drowart, and C. E. Meyers, *J. Chem. Thermo.* **8**, 225 (1976).
- ⁴³Such a large barrier is not improbable. In fact, we have observed an activation barrier of about 4.5 eV in the reaction, $\text{Al}^+ + \text{H}_2 \rightarrow \text{AlH}^+ + \text{H}$ (Ref. 18).
- ⁴⁴K. Morokuma, B. C. Eu, and M. Karplus, *J. Chem. Phys.* **51**, 5193 (1969).
- ⁴⁵M. Menzinger and A. Yokozeki, *Chem. Phys.* **22**, 273 (1977).
- ⁴⁶W. J. Chesnavich and M. T. Bowers, *J. Phys. Chem.* **83**, 900 (1979).
- ⁴⁷R. A. Marcus, *J. Chem. Phys.* **45**, 2630 (1966).
- ⁴⁸The appropriate value of n depends on the energy of the collision. At low energies, the maximum impact parameter leading to reaction is governed by the long-range ion-induced dipole potential. This results in $n = 0.5$. At high energies, the maximum impact parameter is just the hard sphere radii which yields $n = 1$, the line-of-centers function.
- ⁴⁹S. A. Safron, N. D. Weinstein, D. R. Herschbach, and J. C. Tully, *Chem. Phys. Lett.* **12**, 564 (1972).
- ⁵⁰C. E. Klots, *J. Chem. Phys.* **64**, 4269 (1976).
- ⁵¹See, for example, P. J. Robinson and K. A. Holbrook, *Unimolecular Reactions* (Wiley-Interscience, London, 1972).
- ⁵²P. B. Armentrout and J. L. Beauchamp, *J. Chem. Phys.* **74**, 2819 (1981).